



Nickel–Ruthenium Bimetallic Species on Hydrotalcite Support: A Potential Hydrogenation Catalyst

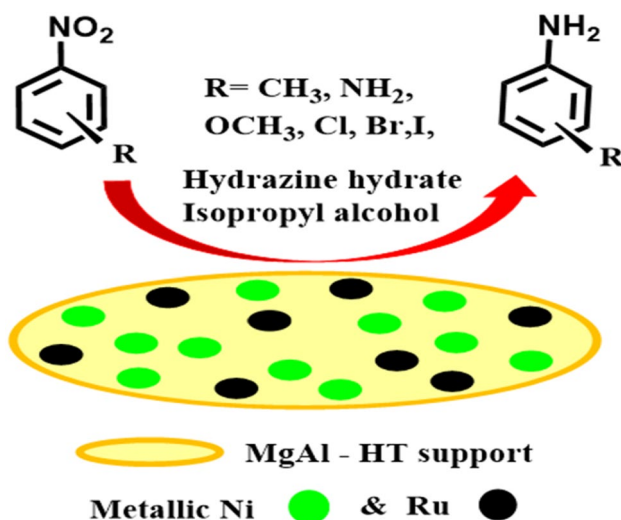
A. Sreenavya¹ · Shabas Ahammed¹ · Arya Ramachandran¹ · V. Ganesh² · A. Sakthivel¹ 

Received: 5 February 2021 / Accepted: 15 May 2021 / Published online: 25 May 2021
© The Author(s), under exclusive licence to Springer Science+Business Media, LLC, part of Springer Nature 2021

Abstract

Nickel–ruthenium loaded on magnesium–aluminium hydrotalcite materials were prepared by a post-synthetic method. The textural and physicochemical properties of the materials were systematically characterised by Fourier transform infra-red (FT–IR), powder X-ray diffraction (XRD), scanning electron microscope (SEM), nitrogen sorption, and X-ray photoelectron spectroscopy (XPS) analysis. The uniform distribution of bimetallic Ni–Ru on hydrotalcite support was evident from the powder XRD and HRTEM analysis of the used catalysts. The hydrogen temperature-programmed reduction profile reveals strong adsorption of hydrogen on the surface of the catalysts. The resultant materials show promising catalytic activity for nitrobenzene reduction under ambient reaction conditions. The formation of metallic nickel and ruthenium on the surface of hydrotalcite under the reaction conditions was evident through powder XRD analysis of the sample obtained under reaction condition. The reaction showed first order kinetics with respect to nitrobenzene. Furthermore, the catalytic activity remained intact for several cycles, and the catalysts also showed promising activity for the reduction of several substituted nitroarene molecules.

Graphical Abstract



Keywords Nitroarenes reduction · Nickel-ruthenium · Hydrotalcite · Catalysts · Layered materials

✉ A. Sakthivel
sakthivelcuk@cukerala.ac.in

Extended author information available on the last page of the article

1 Introduction

The selective reduction of aromatic nitro compounds to corresponding amine derivatives is an industrially important process. Aromatic amines are important raw materials and intermediates in the production of pharmaceuticals, dyes, pigments, agricultural chemicals (pesticides and herbicides), photographic materials, surfactants, textile auxiliaries, polymers (mainly polyurethane), chelating agents, and antioxidants [1–5]. The main challenge in the selective reduction of nitrobenzene to aniline is the formation of toxic phenyl hydroxylamine intermediates, which are unstable and form colored azo and azoxy derivatives [6, 7]. The oldest method used in the industrial production of aromatic amines is the Bechamp reaction, which involves the use of iron and water in the presence of hydrochloric acid to reduce the nitro-group to the amine. However, it has limitations due to serious pollution issues [8]. Now a days, the large-scale manufacturing of aniline is carried out by the catalytic hydrogenation of nitrobenzene over a variety of transition metal-based catalysts such as Ni, Cu, Co, Fe, Ag, Pt, Pd, Ru, etc., either in the liquid phase or vapour-phase as well as electrochemical process [3, 4, 9]. Recently, we have demonstrated NiRu-hydrotalcite-type material for the selective reduction of aromatic nitro compounds to corresponding anilines [10]. However, a comparatively high amount of (≈ 4.2 wt.%) ruthenium present in the catalyst (NiRu-1:0.2) may not be economically viable. In the present study, following the limelight on our previous work, we have attempted to develop environmentally friendly, economically viable hydrogenation catalysts for the selective reduction of nitrobenzene to aniline. In this context, here, nickel ruthenium containing magnesium–aluminum hydrotalcite (MANR) catalysts were prepared by supporting a bimetallic Ni–Ru redox system on a magnesium–aluminium hydrotalcite (HT) support and investigated for the above mentioned reaction. The choice of bimetallic NiRu system on Mg–Al hydrotalcite support was based on the significant properties such as relatively inexpensive and highly abundant nickel and noble metal characteristics of ruthenium [10, 11]. Further, metal oxides derived from hydrotalcite precursors are widely used as potential supports for the dispersion of metal nanoparticles, since they possess excellent adsorption capacity, tunable acidic-basic properties, high surface area, structural stability, etc. [10–18]. Hydrotalcite-derived metal oxides as catalytic supports offer significant benefits for achieving green organic synthesis, potential catalytic activity and selectivity, tolerance of a wide range of reaction conditions, and a simple work-up procedure facilitates easy catalyst recovery and reuse [18–25]. In the present work, a series of nickel-based bimetallic (nickel–ruthenium)

catalysts have been prepared on Mg–Al hydrotalcite support and investigated the activity of the catalysts for the reduction of nitrobenzene and its derivatives.

2 Materials and Methods

2.1 Preparation of MgAl Hydrotalcite Support Having Different MgAl Ratios

Solution A was prepared by dissolving 34.72 mmol of $\text{Mg}(\text{NO}_3)_2$ and 17.48 mmol of $\text{Al}(\text{NO}_3)_3$ in 96 mL of water. Solution B was prepared by dissolving 25.79 mmol of Na_2CO_3 and 125.89 mmol of NaOH in 85.6 mL of water. Solution B was added to Solution A with constant stirring at 60 °C for one hour. The resulting precipitate was allowed to age for 18 h at 60 °C. The precipitate was filtered, washed with deionised water, and dried at 70 °C overnight. The obtained hydrotalcite material with Mg: Al ratio of 2:1 was calcined at 400 °C for 4 h and labelled as MA(2:1). For comparison, MgAl-HT support with different magnesium to aluminium (Mg:Al) molar ratios of 1:1 and 3:1 were also prepared using a similar procedure as described above, and the resultant samples were labelled as MA(1:1) and MA(3:1), respectively.

2.2 Wet-Impregnation of Ni and Ru on the Hydrotalcite Support

The nickel and ruthenium with the molar ratio of 3:1 having good alloying properties [26], which is equivalent to about 2 and 1 wt. % of Ni and Ru respectively were introduced on the surface of Mg–Al hydrotalcite as per the following procedure. A metal salt solution was prepared by dissolving 0.75 mmol of $\text{Ni}(\text{NO}_3)_2 \cdot 6\text{H}_2\text{O}$ and 0.25 mmol of $\text{RuCl}_3 \cdot 3\text{H}_2\text{O}$ in 4.45 mL of water (0.8 mL/g of support). The resultant clear solution was introduced into the support drop by drop with continuous agitation. The wet-impregnated sample was allowed to age at room temperature for 3 h and dried at 70 °C overnight. Then, the sample was calcined at 400 °C for 4 h and labelled as MANR(2:1). For comparison, NiRh and NiIr supported on MgAl hydrotalcite were also prepared using a similar procedure and labelled MANRh(2:1) and MANI(2:1), respectively. The NiRu-supported catalysts were also prepared on the supports with different Mg–Al ratios and labelled as MANR(1:1) and MANR(3:1) respectively.

2.3 Characterization of the Catalyst

FT-IR spectra were recorded on a JASCO-4700 FT-IR spectrometer in the range of 400–4000 cm^{-1} using KBr pellets. These spectra were collected with 4 cm^{-1} resolution and 60

scans in the mid-IR (400–4000 cm^{-1}) region. Powder X-ray diffraction (XRD) analysis of the samples was performed on a Rigaku miniflex (300/600), Japan X-ray diffractometer with Cu-K α radiation ($\lambda = 1.54059 \text{ \AA}$) in the 2θ range of 3–70° with a scan speed and step size of 0.005 min^{-1} and 0.05° min^{-1} respectively. Thermal decomposition of the samples was analysed using a thermal analyser (simultaneous thermal analyser 600, PerkinElmer). Diffuse-reflectance UV–Visible spectra of the samples were recorded on Shimadzu UV-2600 double-beam spectrophotometer with the help of BaSO $_4$ as reference. N $_2$ adsorption–desorption measurements were carried out at –196 °C using an automatic micropore physisorption analyser (Micromeritics ASAP 2020, USA) after the samples were degassed at 150 °C for at least 10–12 h under 0.133 Pascal pressure prior to each run. The Brunauer–Emmett–Teller (BET) surface area was calculated in the relative pressure range of 0.05–0.3, over the adsorption branch of isotherm. A Phillips Technai G 2 T30 scanning electron microscope (SEM) at 300 kV was used to analyse the morphologies and sizes of the resultant materials. Transmission electron microscopy (TEM) images were acquired on a FEI-TECNAI G 2 -20 TWIN with a LaB $_6$ filament. The concentration of nickel and ruthenium present in the fresh and used catalysts were determined using ICP-AES (SPECTRO Analytical, Germany). A custom-built ambient pressure photoelectron spectrometer (APPES; Prevac, Poland) equipped with a VG Scienta R3000HP analyser, and an MX650 monochromator was used for the X-ray photoelectron spectroscopy of the sample. The reducibility of the materials was determined by temperature-programmed reduction (TPR) studies using BELCAT-M (JAPAN). After the catalyst sample was purged with Ar at 100 °C for 30 min, the gas flow (30 mL min^{-1}) was switched to a 5 vol.% H $_2$ in Ar mixture before TPR analysis. The analysis was carried out between 100 °C and 600 °C at a heating rate of 10 °C min^{-1} . Hydrogen consumption was monitored using a TCD detector.

2.4 Hydrogenation Reactions

In a typical catalytic reaction, 2.5 mmol of nitrobenzene was dissolved in 1 mL of isopropyl alcohol (IPA) in a glass batch reactor. About 0.05 g of the catalyst was added to the solution with continuous stirring at 80 °C in nitrogen atmosphere. When the reaction mixture attained the desired reaction temperature, 5 mmol of hydrazine hydrate was added with continuous stirring for 6 h. After the completion of the reaction, the reactor was cooled down to room temperature and the products were extracted with 2 mL of IPA and analysed by gas chromatography (GC) (Mayura Analytical 1100 series gas chromatograph with FID detector, and ZB-5 column (Zebron, 30 m (length) \times 0.32 mm (i.d.), 0.25 μm (film thickness)). The procedure of GC analysis was as follows:

an initial oven temperature was maintained at 70 °C and the oven temperature was ramped at 10 °C min^{-1} until it reached 250 °C and held for 2 min. The conversion of nitrobenzene and the selectivity of the products were calculated based on standard methods using authentic samples. The products were confirmed by gas chromatography coupled with mass spectrometry (GC–MS). Further, the kinetics of the reaction studied by collecting samples at different time interval at various reaction temperature.

3 Results and Discussion

3.1 FT-IR Characterization of the Catalyst

FT-IR spectra of the magnesium–aluminum hydrotalcite (HT) support and various nickel-based bimetallic catalysts on the support are shown in Figs. S1–S3. The supports show three typical IR active vibrations of hydrotalcite-like compounds, i.e. molecular vibrations of hydroxyl groups (3000–3700 cm^{-1}), lattice vibrations of octahedral layers (below 1000 cm^{-1}), and vibrations of interlayer anions (1351 cm^{-1}). The stretching and bending vibrations of hydrogen-bonded hydroxyl groups present in the brucite-like layers can be identified in the region of 3000–3700 cm^{-1} . The bending mode of interlayer adsorbed water molecules appears at approximately 1635 cm^{-1} . Lattice vibrations of the octahedral layers can be observed below 1000 cm^{-1} region of the spectra, which can be assigned to the stretching modes of the Al–O bond (approximately 777 and 551 cm^{-1}) and stretching modes of the Mg–O bond (approximately 661 cm^{-1}). The band found at approximately 1351 cm^{-1} corresponds to the ν_3 mode of the interlayer carbonate (CO $_3^{2-}$) anion. In the fundamental region of 400–1000 cm^{-1} , the wet-impregnated calcined samples show three bands at approximately 835, 792, and 660 cm^{-1} , corresponding to the M–O vibrations of the lattice frame work of octahedral layers [19–21].

3.2 XRD Analysis of the Catalysts

Figure S4 shows the powder XRD patterns of synthesised Mg–Al HT with different Mg/Al molar ratios. All the samples demonstrated well defined reflection patterns of seven characteristic peaks of layered hydrotalcite structure corresponding to (003), (006), (012), (015), (018), (110), and (113) planes at 2θ values of 11.5°, 23.2°, 34.6°, 38.9°, 46.2°, 60.7°, and 62.7° respectively [19–22]. XRD patterns of the corresponding calcined (400 °C for 4 h) samples are shown in Fig. S5. The obtained reflection pattern shows the characteristics of mixed oxide derived from MgAl $_2$ O $_4$ spinel and MgO periclase phases. The characteristic reflections of spinel phase MgAl $_2$ O $_4$ appeared at $2\theta \approx 29.2^\circ$, 31.8° ,

33.2 °, 38.9 °, 47.6 °, 59.4 °, and 64.4 ° with a contribution of MgO periclase phase at $2\theta \approx 35.2^\circ$, 43.1° , and 62.3° respectively [19–23].

Figure 1 shows the XRD patterns of NiRu on MgAl-HT support. The X-ray reflection of the NiRu supported on MgAl-HT exhibits XRD patterns similar to those of MA samples. The obtained pattern shows the peaks corresponding to Mg(Al,Ni)O periclase at $2\theta \approx 35.5^\circ$, 43° , and 62.5° with the presence of MgAl₂O₄ or NiAl₂O₄ spinel phase. The absence of any reflections corresponding to the RuO_x can be attributed to the uniform distribution of ruthenium species in the form of solid solution with nickel on the surface of HT matrix [24, 25, 27, 28]. Figure S6 shows the powder XRD patterns of the catalysts prepared with NiRu, NiRh, or NiIr on MgAl-HT support. Figure S6 shows that all the samples exhibit presence of hydrotalcite, MgAl₂O₄ spinel, and Mg(Al,Ni)O periclase phases. In all these cases, there is no segregated bulk oxide, which indicates the uniform distribution of nickel and noble metal ions on the surface of hydrotalcite support [24, 25, 27, 28].

3.3 Textural Properties of the Materials Using BET and SEM Analysis

Figure 2 shows the N₂ adsorption–desorption isotherms of the bimetallic nickel catalysts on the HT support. MANRh (2–1) and MANI (2–1) exhibit type IV isotherms with H3-type hysteresis, which is characteristic of porous solids with non-rigid aggregates of plate-like particles with slit-shaped pores. The MANRWC sample exhibits a type IVa isotherm with a H2b hysteresis loop, which is associated with mesoporous solids with a complex network-type pore structure [29, 30]. Specific surface area values of these materials are summarized in Table 1, which are all in the range

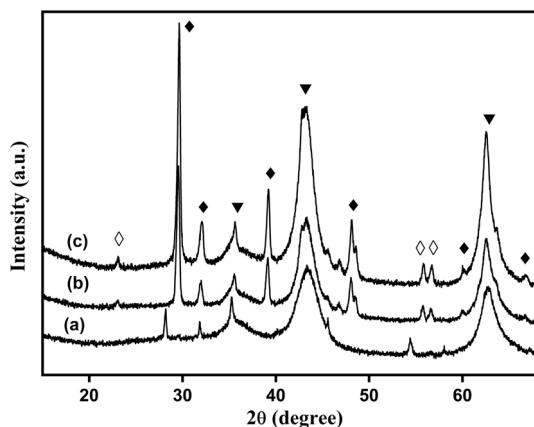


Fig. 1 Powder XRD pattern of (a) MANR (1:1); (b) MANR (2:1); (c) MANR (3:1). (White filled diamond)HT; (Black filled diamond) MgAl₂O₄ or NiAl₂O₄ spinel; (Black filled downward triangle) Mg(Al,Ni)O periclase

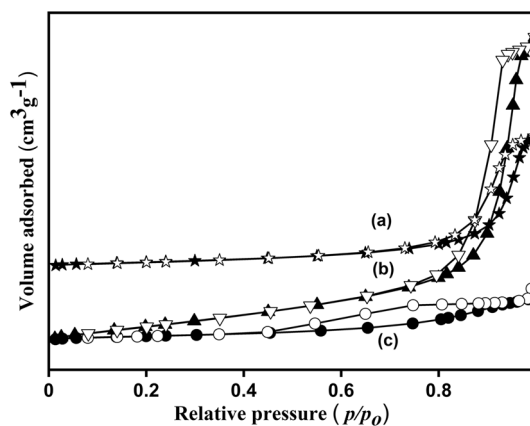


Fig. 2 Nitrogen sorption isotherms of (a) MANR(2:1), (b) MANRh(2:1) and (c) MANI(2:1) (filled symbols represent adsorption and open symbols represent desorption)

of the hydrotalcite matrix. SEM images of the nickel–ruthenium, nickel–rhodium, and nickel–iridium on the Mg–Al HT support are shown in Fig. S7. All the samples exhibited non-uniform distribution of particles with irregular morphology.

3.4 XPS Investigation of the Catalysts

The surface oxidation states of the metal ions present in the synthesised materials were determined by XPS measurements. Figure 3 shows the XPS results of the Ni 2p core level spectra of the MANR (2:1), MANRh (2:1), and MANI (2:1). The binding energies of Ni 2p_{3/2} and Ni 2p_{1/2} appear very similar in all these samples. The Ni 2p spectrum of all the samples consists of a main peak of Ni 2p_{3/2} at the binding energy value of 855.8 eV with a broad satellite peak at 861.9 eV, whereas the Ni 2p_{1/2} located at the binding energy value of 873.6 eV with a satellite peak at 879.7 eV. The observed binding energy values could be assigned to the species of Ni²⁺ (NiO), strongly interacting with the magnesium–aluminium HT support [10, 27].

Similarly, the XPS profiles of Ru, Rh, and Ir species present in the materials are shown in Fig. 4. It can be observed that Ru 3d_{3/2} peak exhibits a binding energy value of 285 eV, which corresponds to the hydrated RuO₂ present in the Mg–Al HT-based support. Similarly, the Ir 4f core level

Table 1 Textural properties of the supported catalysts

Catalyst	BET surface area (m ² g ⁻¹)	Pore volume (cm ³ g ⁻¹)	Average pore size (nm)
MANR(2:1)	41.9	0.131	12.5
MANRh(2:1)	164.9	0.753	18.2
MANI (2:1)	54.8	0.324	23.6

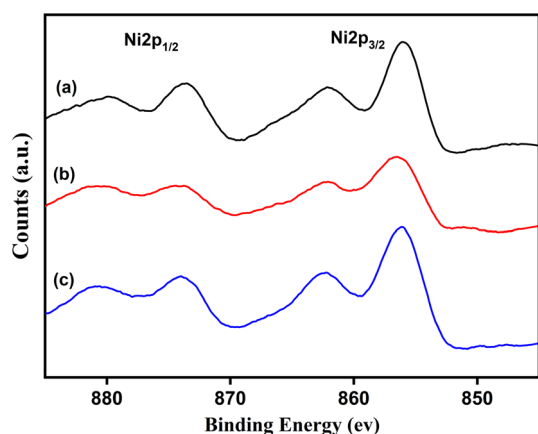


Fig. 3 XPS of Ni 2p in (a) MANR (2:1), (b) MANRh(2:1) and c MANI (2:1)

spectra of the MANI (2:1) sample shows a prominent peak of Ir $4f_{7/2}$ at the binding energy of 63.1 eV, indicating the presence of Ir in the +3 oxidation state. The Rh $3d_{5/2}$ spectrum for the MANRh (2:1) sample shows the peak at the binding energy value of 305.36 eV with a satellite peak at 309.85 eV and can be assigned to trivalent rhodium species present in the surface of the support [10, 27, 31, 32].

3.5 TPR Analysis of the Catalysts

TPR profiles of various MANR samples are shown in Fig. 5. The redox properties of MANR materials prepared with different Mg–Al ratios were studied using TPR with hydrogen. TPR studies can help us to understand the most suitable reduction conditions for supported bimetallic nickel–ruthenium catalysts. The presence of a single asymmetric peak in the temperature range of 400–600 °C suggests the presence of a uniform distribution of bimetallic Ni–Ru on the surface of the HT support. It is observed that the increase in the Mg–Al ratio increases the shift in the reduction peak

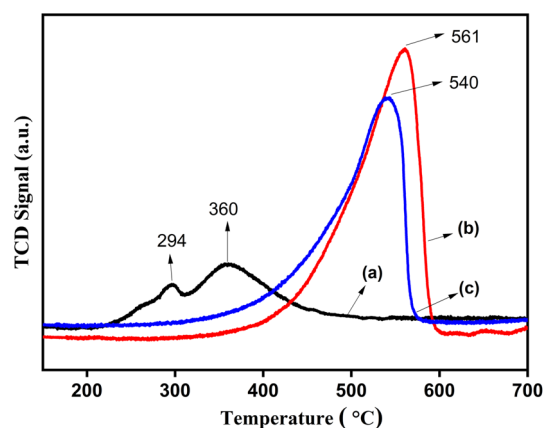


Fig. 5 TPR profiles of (a) MANR (1:1), (b) MANR (2:1) and c MANR (3:1)

towards the higher temperature region. This suggests that a decrease in the aluminium content in the MgAl-HT support facilitates strong basic sites, which further increases the metal–support interaction. The sample MANR (2:1) shows the highest reduction temperature, which can be attributed to the strong basicity of the sample resulting in strong interactions with Ni^{2+} and Ru^{n+} ions introduced by the wet impregnation method. The sample MANR (1:1) has the lowest metal reduction temperature and shows two distinguishable reduction peaks corresponding to the non-uniform distribution of nickel and ruthenium ions present on the support [10, 26, 33].

Figure S8 shows the TPR profile of various nickel-based bimetallic (Ni–Ru, Ni–Rh, and Ni–Ir) catalysts. Among the various catalysts, MANRh(2:1) shows the lowest reduction temperature in the range of 423 °C. The lowest reduction temperature may be attributed to the weakest interaction of nickel–rhodium ions with the support. Moreover, MANI(2:1) and MANR (2:1) samples exhibit higher reduction temperatures in the range of 550 °C, indicating their strongest interaction with the support [10, 26, 33].

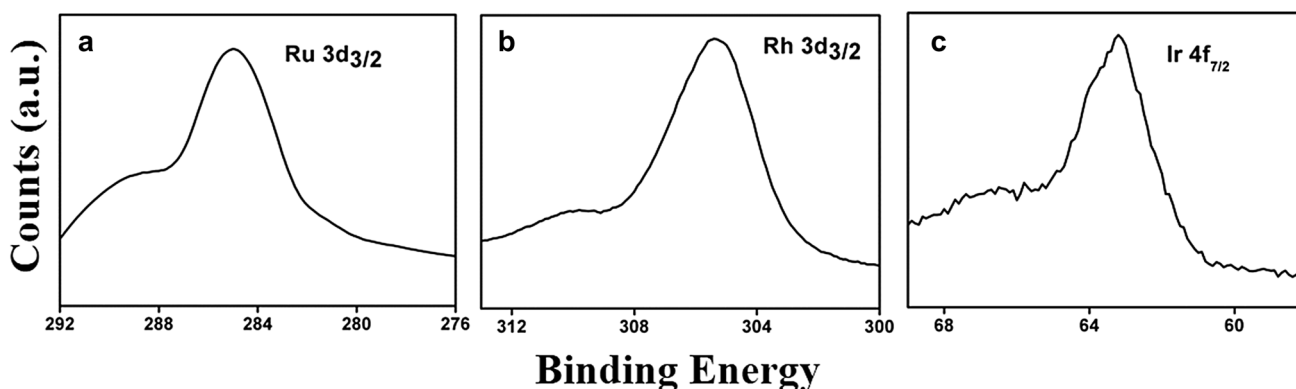


Fig. 4 XPS spectra of a MANR (2:1) for Ru 3d level and b MANRh (2:1) at Rh 3d level and c MANI(2:1) for Ir 4f level

4 Catalytic Reduction of Nitrobenzene Using Various Catalysts

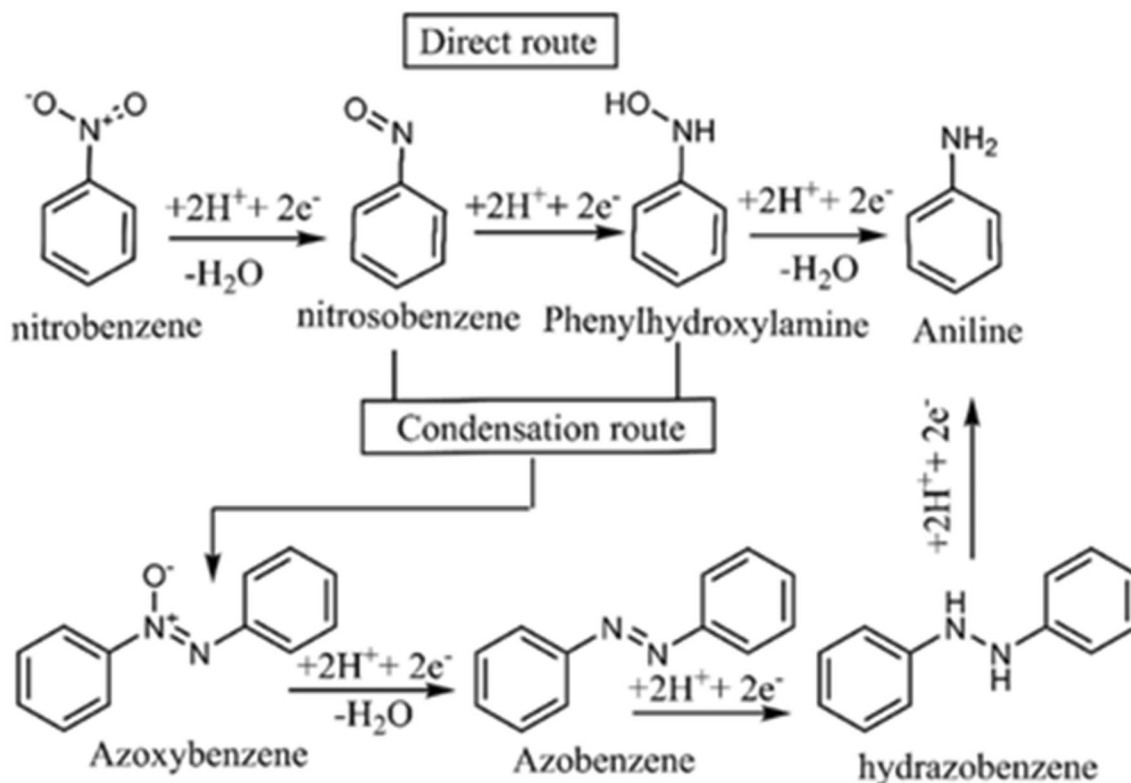
The resultant nickel-based bimetallic catalysts were explored for the reduction of nitrobenzene to aniline with hydrazine hydrate as the hydrogen source and isopropyl alcohol as the solvent (Scheme 1). The results are summarized in the following section.

The reduction of nitrobenzene can take place in several ways, i.e. either through direct route via the formation of nitrosobenzene and phenylhydroxylamine as intermediates or through a condensation route via the formation of azoxy benzene, azobenzene, and hydrazobenzene as intermediates. The condensation route is favoured under basic conditions. In the present study, NiRu, NiRh and NiIr supported on magnesium–aluminium hydrotalcite support gives aniline as the major product with a considerable amount of azoxybenzene and azobenzene as the by-products, thereby demonstrating that the reduction of nitrobenzene proceeds through the condensation route due to the basicity offered by the magnesium–aluminium hydrotalcite support of the catalysts [10, 34–37].

4.1 Performance of Various Nickel-Based Bimetallic Catalysts on MgAl Hydrotalcite Support Having Different Mg/Al Ratios on the Reduction of Nitrobenzene

Our initial efforts were focused on the reduction of nitrobenzene using various nickel-based bimetallic catalysts, and the results are shown in Table 2.

Among the various catalysts studied, Ru and Rh on MgAl–hydrotalcite support with different Mg/Al ratios, affording a complete conversion of nitrobenzene, and Ni–Ir based catalyst shows comparatively less conversion. Among all the catalysts supported on MgAl–hydrotalcite support, those with Mg/Al ratio of 2:1 showed better conversion and selectivity to aniline under the optimum reaction conditions. The optimum basicity offered by the support compiled with the redox properties of the bimetallic system may facilitate better nitroarene conversion and aniline selectivity. The oxyanion present on the surface of hydrotalcite support facilitate to interact with nitrogen center of the nitrobenzene, which enhances the electron density in the oxygen centers of nitrobenzene and facilitate the abstraction of protons from the metal surface (Scheme 2). Bimetallic nickel–rhodium supported catalysts show a complete conversion with high selectivity to aniline, irrespective of the Mg/Al ratio of the support. The synergic effect of bimetallic Ni–Rh system on



Scheme 1 Possible reaction pathways for the reduction of nitrobenzene [10, 36, 37]

Table 2 Reduction of nitrobenzene using various nickel-based catalysts[‡]

Catalyst	% Conversion	% Selectivity aniline	% Selectivity azobenzene	% Selectivity azoxybenzene
MANR(1:1)	100	55.5	15.8	28.5
MANR(2:1)	100	68.3	18.9	12.7
MANR(3:1)	100	33.2	28.4	38.4
MANRh(1:1)	100	87.9	10.5	1.5
MANRh(2:1)	100	90.4	8.5	1.1
MANRh(3:1)	100	74.2	16	9.7
MANI(1:1)	33.9	96.9	0.5	2.5
MANI(2:1)	67.3	62.2	4.9	32.9
MANI(3:1)	27.4	100	0	0
NiRu/Al ₂ O ₃	51.5	68.4	8.8	22.8
NiAl – HT	58.5	86	2.2	11.7

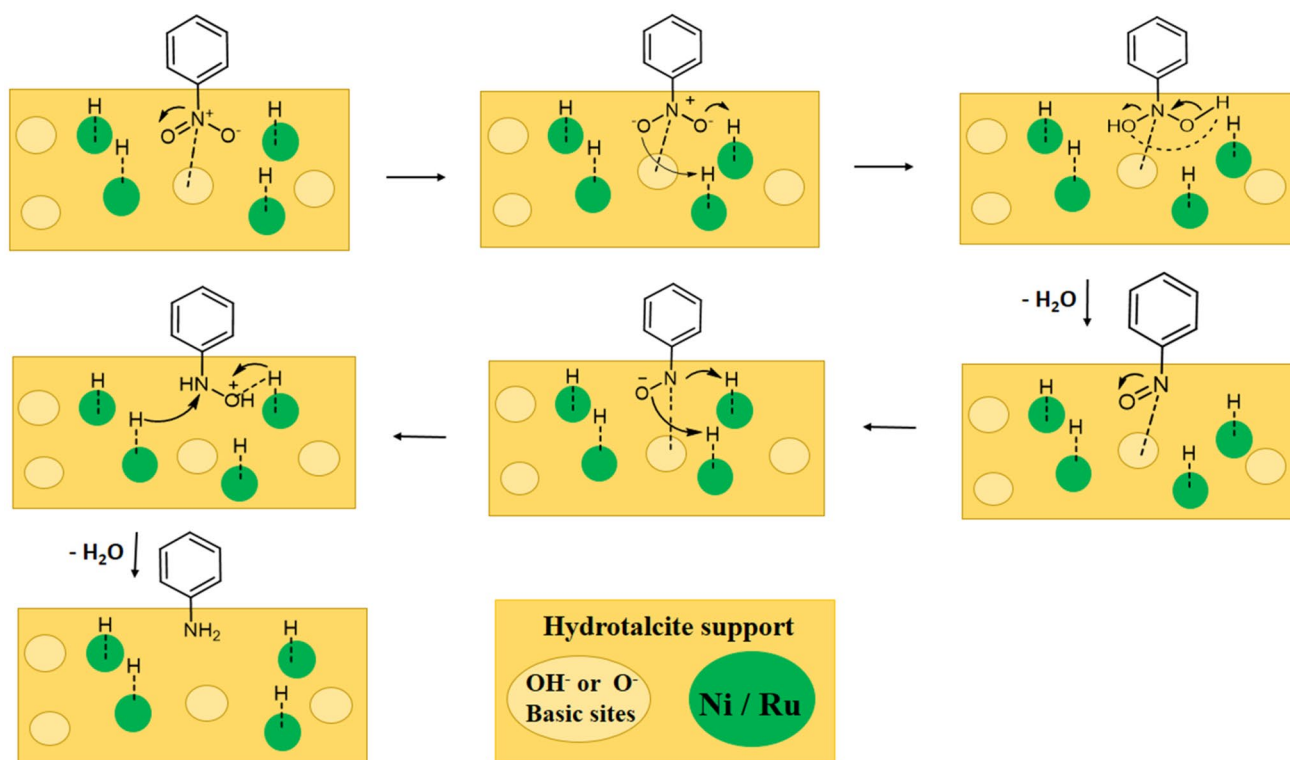
[‡]Reaction conditions: Nitrobenzene 2.5 mmol, hydrazine hydrate 5 mmol, catalyst 0.05 g, T = 80 °C and t = 6 h

basic Mg/Al hydrotalcite support may help in controlling the release of hydrogen by the decomposition of hydrazine hydrate, which may favour the complete conversion with the exclusive formation of aniline. However, the higher cost of rhodium is the main drawback for its large-scale use; therefore, our focus has been devoted to the next best system,

i.e. nickel–ruthenium on Mg/Al HT support. In the present study, the MANR catalyst contains nickel and ruthenium in the molar ratio of 3:1 and are supported on the surface of Mg–Al hydrotalcite. The basis for selecting the typical catalyst composition was the superior catalytic activity of NiRu-hydrotalcite type materials possessing nickel and ruthenium in the molar ratio of 3:1 for the hydrogenation of biomass model compounds and nitroarenes as well as their high alloying properties [10, 26]. Nickel–ruthenium on MgAl-HT support with Mg/Al ratio of 2:1 (MANR (2:1)) resulted in complete conversion of nitrobenzene with 68% selectivity to aniline in the presence of a considerable amount of azoxy and azobenzene as the side products. Furthermore, all these studies have been carried out using a MANR (2:1) catalyst. Bimetallic Ni–Ru on acidic support (NiRu/Al₂O₃) showed only 51% conversion of nitrobenzene. The reaction did not proceed without the catalyst, which showed only less than 1% conversion.

4.2 Influence of the Volume of Solvent on the Conversion of the Reaction

The catalytic activity of the MANR (2:1) sample was further studied using different volumes of solvent (isopropanol). The results of our study are depicted in Fig. 6.



Scheme 2 Plausible mechanism of the hydrogenation of nitrobenzene over the surface of MANR (2:1) catalyst

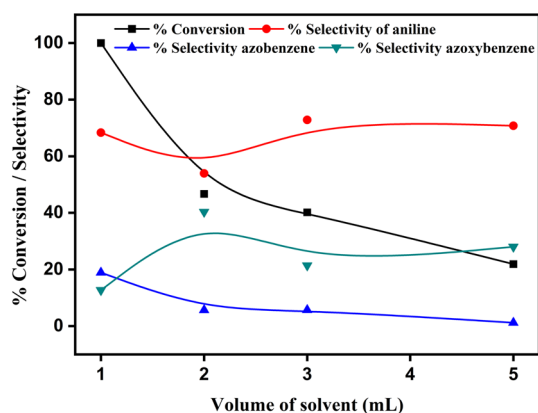


Fig. 6 Effect of volume of solvent on the reduction of nitrobenzene[‡]. [‡]Reaction conditions: nitrobenzene 2.5 mmol, hydrazine hydrate 5 mmol, catalyst=0.05 g, T=80 °C and t=6 h

It can be noticed from Fig. 6 as the volume of the solvent increases, the conversion of nitrobenzene steadily decreases. The use of a minimum solvent facilitates better substrate-active site interactions, resulting in complete nitrobenzene conversion with 68% aniline selectivity. The preferential adsorption of hydrogen species obtained from hydrazine hydrate is the first step in the reduction of nitrobenzene [38]. The concentration of adsorbed hydrogen species on the catalyst surface and accessibility of the reactant to the catalyst surface demonstrate a decrease in the presence of a large solvent volume. The competitive adsorption of solvent on the active surface could likely be the reason for the low conversion of nitrobenzene when a large volume of solvent was used. Therefore, in order to retain the maximum conversion and selectivity, all the reactions were carried out in 1 mL of isopropanol.

4.3 Evaluation of Various Solvents on the Reduction of Nitrobenzene

The catalytic activity of MANR(2:1) using different solvents was investigated. The results of our investigation are shown in Fig. 7.

The polarity index of the solvents used in the present study is in the order: hexane < toluene < isopropanol < dimethylformamide (DMF). As can be seen in Fig. 7 the extremely polar and protic nature of DMF solvent (polarity index 6.4) yields a less conversion. The use of other solvents such as isopropanol, toluene and hexane, increased the conversion with increasing polarity of the solvents. The use of the least polar solvent i.e. hexane (polarity index 0.1), yielded 56% conversion with selective formation of aniline as the product. In the presence of non-protic moderate polar solvent like toluene (polarity index 2.4), the reaction showed 76% conversion with 63% aniline selectivity and with the formation of a

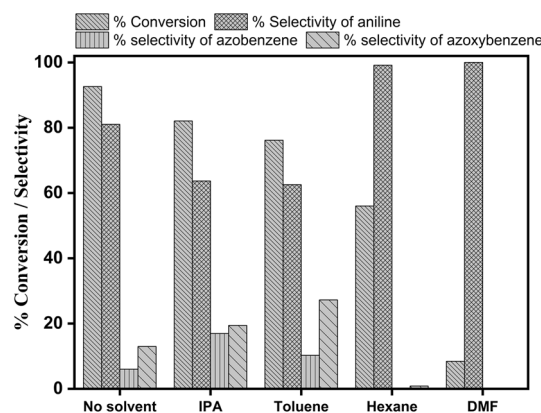


Fig. 7 Evaluation of different solvents on the reduction of nitrobenzene[‡]. [‡]Reaction conditions: nitrobenzene 2.5 mmol, solvent 1 mL, hydrazine hydrate 5 mmol, catalyst=0.05 g, T=80 °C and t=6 h

considerable amount of azo and azoxy byproducts. Isopropanol with a polarity index of 3.92 resulted in complete conversion of nitrobenzene with 68% selectivity to aniline and a considerable amount of azo and azoxy byproducts. It can be concluded that the use of protic polar solvent does not favour the reaction, whereas *iso*-propanol, with optimum polarity, as the solvent facilitates a complete conversion. The formation of azo and azoxy byproducts was negligible when a less polar solvent (hexane) was used for the reaction. Among the various solvents studied (hexane, toluene, *isopropyl* alcohol and dimethylformamide), *isopropyl* alcohol has the lower reduction potential and can act as optimum hydrogen donor under the reaction condition and facilitates better conversion for nitroarene reduction [39]. The reduction of nitrobenzene was also carried out without a solvent which yielded a better conversion of 93% with 81% selectivity to aniline. The improved nitrobenzene conversion and selectivity to aniline can most likely be attributed to the free accessibility of hydrogen species on the active sites of the catalyst and the ease of accessibility of the reactant to the catalyst surface in the absence of solvent. Therefore, to improve the selectivity to aniline, all the reactions were carried out without using any solvent.

4.4 Effect of Hydrazine Ratio on the Reduction of Nitrobenzene

To understand the role of *isopropyl* alcohol as a hydrogen source, first the reaction has been carried out without using the hydrazine hydrate and it is observed that the reaction does not proceed further. This may be because under the mild reaction condition, *isopropyl* alcohol may not be able to act as a hydrogen donor. In order to improve the selectivity of aniline, the reaction was further explored by varying the amount of hydrogen source, that is, hydrazine hydrate,

and the results are shown in Fig. 8. It can be observed from Fig. 8 that the conversion of nitrobenzene and selectivity of aniline increased with increasing ratio of hydrazine. The reaction carried out using nitrobenzene-to-hydrazine ratio of 1:3 yielded 100% conversion with 82% selectivity to aniline. The selectivity of aniline remains almost unchanged on further increasing the nitrobenzene-to-hydrazine ratio.

4.5 Effect of Substrate-to-Catalyst Ratio in the Reduction of Nitrobenzene

The reaction was also studied by varying the substrate-to-catalyst ratio, as shown in Fig. 9. As the substrate-to-catalyst ratio increased, the conversion of the reaction decreased. When the substrate-to-catalyst molar ratio was 120, the reaction showed 100% conversion with 68.3% selectivity of aniline. The reaction showed better conversion (92.6%) with improved selectivity (81%) to aniline when the substrate-to-catalyst ratio was 240. A further increase in the substrate-to-catalyst ratio drastically decreased the conversion (67%).

4.6 Reduction of Nitrobenzene Using Various Bimetallic Catalysts

In order to understand the importance of NiRu bimetallic system for nitrobenzene reduction, the reaction was studied using bare hydrotalcite, monometallic nickel, and ruthenium supported on HT, and these results were compared with that of MANR (2:1) catalyst. The results are summarized in Fig. 10. The bare magnesium–aluminum hydrotalcite support shows only 49% conversion of nitrobenzene with 60% aniline and 37.1% azoxybenzene and 2.8% azobenzene as the products. Nickel impregnated MgAl-hydrotalcite support

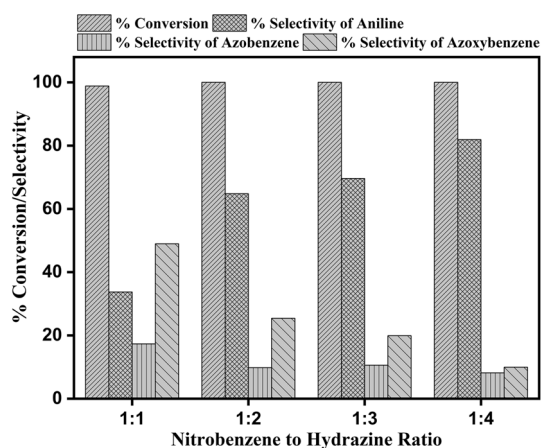


Fig. 8 Effect of nitrobenzene to hydrazine ratio on the reduction of nitrobenzene[‡]. [‡]Reaction conditions: nitrobenzene 2.5 mmol, hydrazine hydrate 2.5 mmol, 5 mmol, 7.5 mmol and 10 mmol, catalyst = 0.05 g, T = 80 °C and t = 6 h

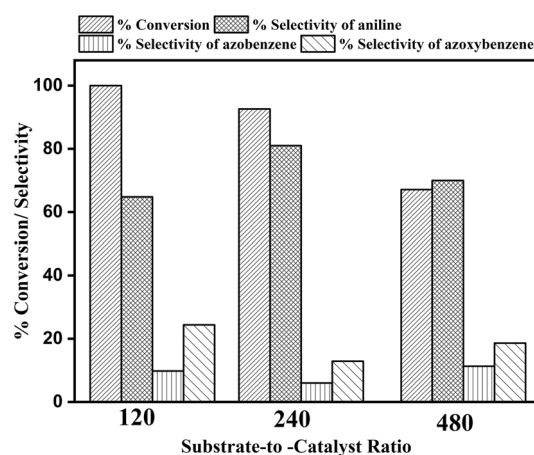


Fig. 9 Effect of substrate to catalyst ratio in the reduction of nitrobenzene[‡]. [‡]Reaction conditions: Nitrobenzene 2.5 mmol, hydrazine hydrate 5 mmol, T = 80 °C and t = 6 h

catalyst showed 66% nitrobenzene conversion with 90% aniline selectivity. Ruthenium impregnated on the MgAl-hydrotalcite support catalyst showed 56% conversion of the reaction with 76% aniline selectivity. Bimetallic NiRu impregnated magnesium–aluminium hydrotalcite support catalyst showed 92% conversion with 81% selectivity for aniline. The synergistic effect of the bimetallic Ni-Ru catalyst on the Mg–Al hydrotalcite support showed better nitrobenzene conversion than the monometallic catalysts. The ruthenium species present in the catalyst support may be reduced at the reaction temperature and promotes the reduction of nickel species present in the catalyst surface by hydrogen spillover effect [26]. The synergistic effect of the bimetallic nickel-ruthenium system combined with the optimum basicity offered by the magnesium–aluminium hydrotalcite support might be the cause for the observed higher

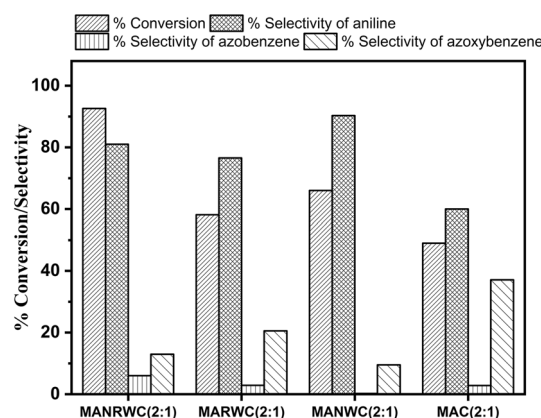


Fig. 10 Reduction of nitrobenzene over various catalysts[‡]. [‡]Reaction conditions: Nitrobenzene 2.5 mmol, hydrazine hydrate 5 mmol, catalyst 0.05 g, T = 80 °C and t = 6 h

conversion and improved aniline selectivity in the presence of MANR(2:1) catalyst [10, 26].

4.7 Kinetic Study on MANR (2:1) Catalyst

The kinetic studies on nitrobenzene hydrogenation on the surface of MANR(2:1) catalyst were carried out under the optimized reaction condition in which complete conversion of nitrobenzene takes place with maximum selectivity (2.5 mmol nitrobenzene, 7.5 mmol hydrazine hydrate (nitrobenzene-to-hydrazine ratio of 1:3), 0.05 g catalyst, and without using a solvent). The initial rate of the reaction was calculated at 50 °C, 60 °C, and 70 °C and the results are presented in Fig. 11. At low temperature (50 °C), the conversion gradually increases with time, reaching a maximum of about 4.65% after around 40 min. An increase in reaction temperature (70 °C) leads to about 20% conversion being obtained within 40 min. The rate of the reaction was steadily increases with increase in reaction temperature. The reaction appears to be first order with respect to nitrobenzene. The apparent activation energy (E_a) was found to be 56.53 kJ/mol from the Arrhenius plot by plotting $\ln(k)$ versus $1/T$, which is comparable to the values reported in literature [40–43].

4.8 Characterization of the Used Catalyst

Further to understand the structure and property relationship of the catalyst, the used catalysts were characterized by powder XRD and HR-TEM analysis, UV–Vis spectroscopy and TGA analysis, and the results are described in the following section.

The powder XRD pattern of the used MANR (2:1) catalyst reveals the retention of layered HT structure under the reaction conditions (Fig. 12). Further, in order to identify the actual active species involved during the reaction, the catalyst was treated with hydrazine hydrate under the reaction condition

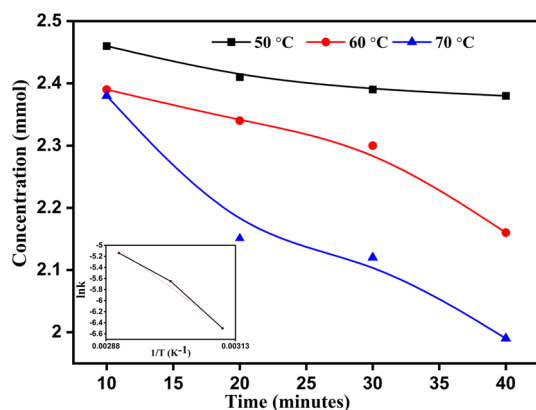


Fig. 11 Effects of temperature and time on the hydrogenation of nitrobenzene over MANR(2:1) catalyst

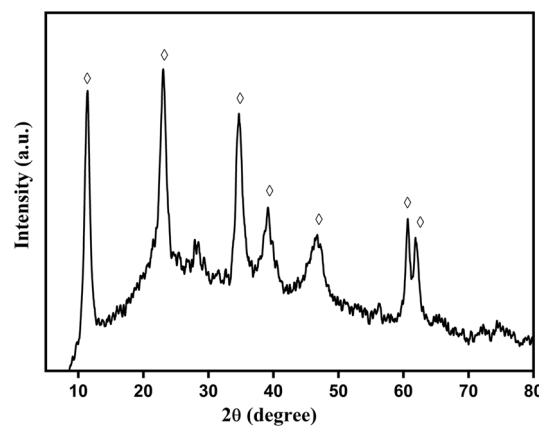


Fig. 12 XRD analysis of the used MANR (2:1) catalyst. (White filled diamond) HT phase

and powder XRD pattern of the corresponding sample was followed and the result is shown in Fig. 13. The catalyst shows X-ray reflection corresponds to (003), (006), (009), (110) and (113) planes at 2θ values 11.27 °, 22.69 °, 34.47 °, 60.4 °, and 61.7 ° which are characteristics of layered hydrotalcite structure. The above fact support that the catalyst retaining its layered structure under the reaction conditions. The catalysts also showed an additional broad peak centered at 38.6 ° and 42.7 ° which can be assigned as (100) and (002) planes of metallic ruthenium species formed under the reaction conditions and dispersed on the hydrotalcite support [10, 26, 44]. The morphology (Fig. 14) of the used catalyst shows lattice fringes corresponding to a layered structure in the presence of nanosized metallic species dispersed on the HT-layer. Both the studies revealed that the synergic effect of *in-situ* formed metallic nanoparticles (NiRu–nanoparticles) on the HT surface might be the active species for the chosen catalytic reaction [10, 26]. The metal composition present in the fresh and used MANR(2:1) catalysts were obtained from ICP-AES studies,

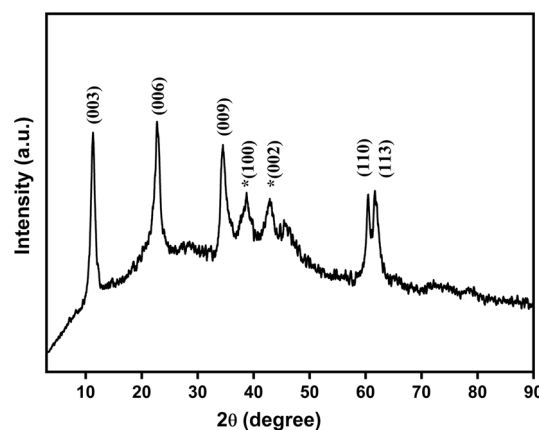


Fig. 13 Powder X-ray diffraction (XRD) pattern of MANR(2:1) sample under the reaction condition

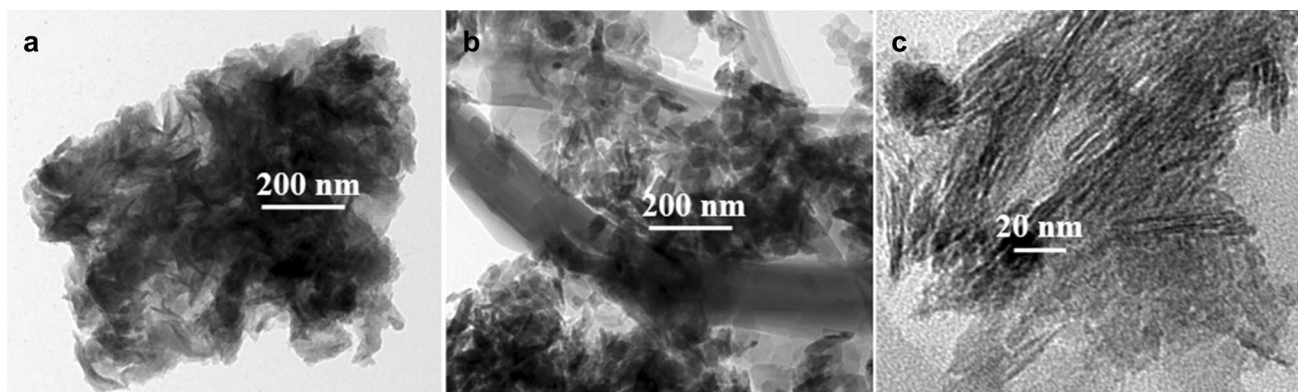


Fig. 14 TEM Images of used **a** MANR (2:1), **b** MANRh (2:1) and **c** MANI (2:1) catalysts

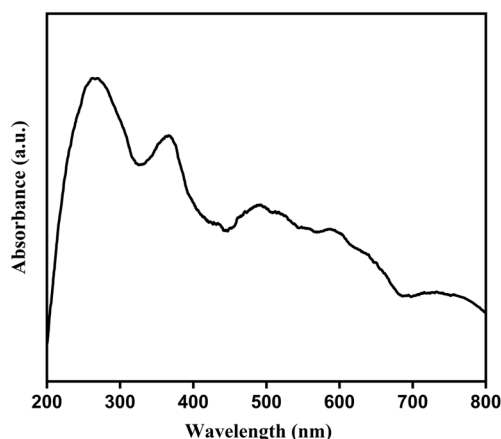


Fig. 15 DRUV-Visible spectrum of used MANR (2:1) catalyst

which reveals that the fresh catalyst contains 1.85 and 1.06 wt.% of nickel and ruthenium respectively. The corresponding used catalyst contains 1.79 and 1.03 wt. % nickel and ruthenium, which clearly evident that the active metal species were stable and retain on the surface of hydrotalcite support under the reaction conditions. Further, the oxidation status of the metal species present in the used catalysts were analysed using DRUV-Vis spectrum and the result is displayed in Fig. 15. The UV-Visible spectrum of recycled catalyst showed three absorption maxima in the wavelength region of 263 nm, 365 nm, and 590 nm (Fig. 15) corresponds to the electronic transition characterization of octahedral Ni^{2+} species present in the used catalyst [10]. The catalyst actually existed in an oxidized state, they could be reduced by hydrazine hydrate under the reaction conditions which is evident from the powder X-ray diffraction (XRD) pattern of MANR(2:1) sample under the reaction condition (Fig. 13) and the TEM analysis (Fig. 14) of used MANR(2:1) catalyst. The *in-situ* forming metallic species (nickel and ruthenium) under the reaction condition might be the active species for the reduction reaction of nitrobenzene.

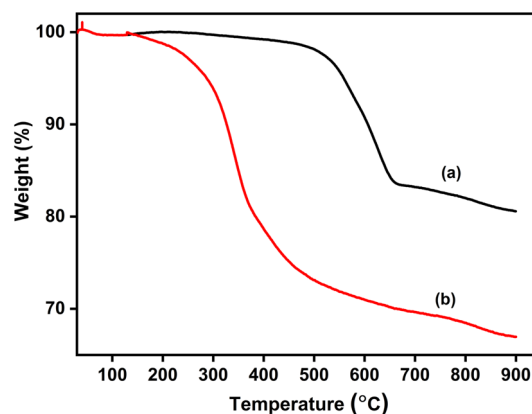
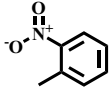
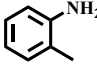
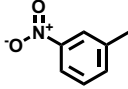
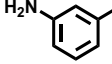
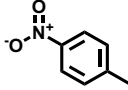
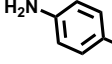
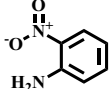
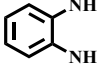
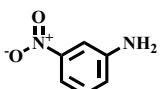
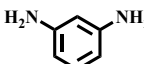
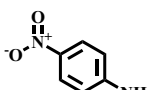
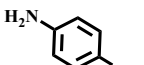
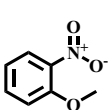
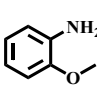
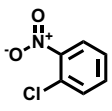
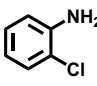
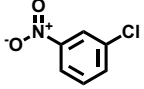
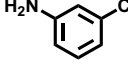
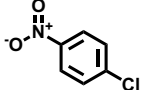
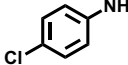
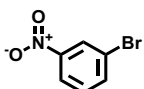
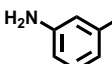
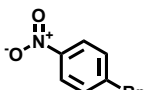
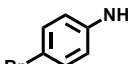
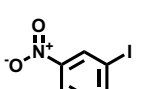
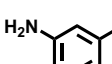


Fig. 16 TGA profile of **a** fresh MANR (2:1) **b** used MANR (2:1) catalyst

As the number of cycles increases the reducibility of the catalyst may decrease and some of the active species may exist in its oxidized state, which is evident from the UV-Vis spectra of the used catalyst. This change in the oxidation state of the metal could be one of the the reason for the slight decrease in the activity of the recycled catalyst. In addition, to investigate the adsorption of organics on the surface of the catalyst after the reaction, thermo gravimetric (TG) analysis was performed to evaluate the degree of adsorption and the results are displayed in Fig. 16. Both the fresh and used catalysts do not showing weight loss before 150 °C. The used catalyst shows a rapid weight loss in the temperature range of 150–450 °C, which is mainly caused by the burning of adsorbed organics on the catalytic surface. The weight loss in the range of 150–450 °C between the used (25%) and fresh catalysts (1%) reflects the amount of adsorbed organic molecules on the catalyst surface. The fresh catalyst shows a weight loss after 450 °C which may be due to the decomposition of crystalline carbon from the carbonate present in the material, since the gasification of amorphous carbon takes place below 400 °C [45, 46].

Table 3 Influence of the substituents on the reduction of nitro-arene[‡]

Sl. No	Substrate	Conversion (%)	Product	Selectivity (%)
1		100		86.2
2		100		96.3
3		100		100
4		100		100
5		100		100
6		100		100
7		82.6		100
8		–		–
9		–		–
10		46.7		100
11		2		100
12		41.2		100
13		2.2		100

[‡]Reaction conditions: MANR (2:1) 50 mg, 0.5 mmol substrate, 5 mmol Hydrazine, 1 mL IPA, 80 °C, 6 h

4.9 Influence of Substituents on the Reduction of Nitrobenzene

To evaluate the influence of substituents on the nitroarene reduction, a variety of substituted nitroarenes to

corresponding amines were studied using the MANR(2:1) catalyst, and the results are summarized in Table 3.

It is observed that better conversion is achieved when an electron-donating group is attached to the nitroarene ring. Irrespective of the position of the substituents (nitrotoluene

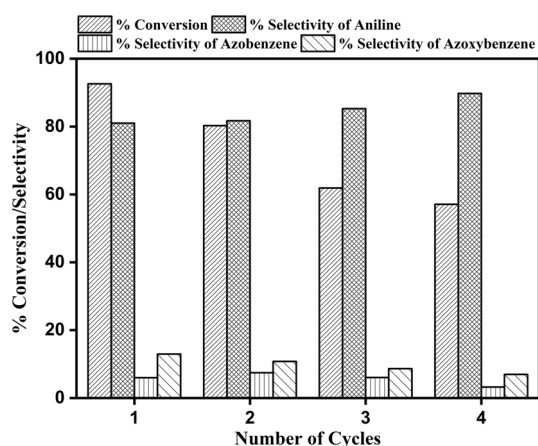


Fig. 17 Recycling ability of MANR (2:1) catalyst in the reduction of nitrobenzene[‡]. [‡]Reaction conditions: Nitrobenzene 2.5 mmol, hydrazine hydrate 5 mmol, catalyst 0.05 g, T = 80 °C and t = 6 h

and nitroaniline) showed complete conversion with better selectivity to the corresponding amine on reduction using the MANR(2:1) catalyst. 2-nitroanisole gave 83% conversion with 100% selectivity to the corresponding amine product. Electron-withdrawing substituents on the nitrobenzene ring decrease the reduction rate. The presence of electron-withdrawing groups (halogens) at the *para* position gives better conversion than its *meta* isomer. This can be explained based on the *ortho-para* directing nature of the halide ions due to their resonance stabilization. It is interesting to note that the usual side products azoxy and azo compounds were not observed or negligible in the reduction of substituted nitrobenzene.

4.9.1 Recyclability Study of the Catalyst

Easy recovery of the catalyst from reaction mixtures and reusability are the significant advantages of heterogeneous catalysts for their large-scale industrial usage. The stability of the MANR(2:1) catalyst was studied for the reduction of nitrobenzene under identical reaction conditions. After each experimental run, the reaction products were extracted using isopropanol, washed several times with IPA, dried overnight at 120 °C, and used for the subsequent run. The procedure was repeated for four cycles, and the results are depicted in Fig. 17. The results show that the catalytic activity gradually decreases in the initial runs and is almost constant after the 3rd run. The gradual decrease in conversion in the initial stage may be due to the change in the oxidation state of the metal ions on the catalyst support, which is evident from the UV–Vis spectrum of the used catalyst or due to the adsorption of organics on the active sites of the catalyst, which is evident from the TGA profile of the used catalyst. Although

the catalyst shows a reduction in conversion, the selectivity of aniline remains constant in all the cycles.

5 Conclusion

Bimetallic Ni-Ru, Ni-Rh, and Ni-Ir on magnesium-aluminum hydrotalcite support catalysts were prepared using a wet-impregnation method and their catalytic activity for the reduction of nitrobenzene was explored. Among the several catalysts studied the Nickel-ruthenium bimetallic species on HT support (MANR(2:1)) catalyst shows a complete conversion of nitrobenzene with good aniline selectivity (68%). The selectivity of aniline was improved to 81% by neat reaction (without solvent) on MANR (2:1). Azobenzene and azoxybenzene were formed as byproducts. The nickel-rhodium containing HT support (MANRh) showed complete conversion of nitrobenzene with similar selectivity of aniline. However, the nickel-iridium containing HT (MANIWC) catalyst was the least active for the reduction of nitrobenzene under identical conditions. Recyclability studies showed that the activity of the MANR (2:1) catalyst decreased slightly in each cycle, but the selectivity of aniline remained unchanged. Further, the catalyst was found to effectively convert the several substituted nitroarene molecules. The XRD and TEM analysis of used catalyst revealed the in-situ formation of metallic Ni-Ru species as an active species.

Supplementary Information The online version contains supplementary material available at <https://doi.org/10.1007/s10562-021-03673-x>.

Acknowledgements The authors thank DST-SERB-CRG (Project No.: CRG/2019/004624) for financial support. A. Sreenavya is grateful to CUK for the fellowship and necessary Lab facilities.

CSIR – CECRI Manuscript Communication Number: CECRI/PESVC/Pubs./2021–066.

Declarations

Conflict of Interest There are no conflicts to declare.

References

- Varkolu M, Velpula V, Pochamoni R, Muppala AR, Burri DR, Kamaraju SRR (2016) Nitrobenzene hydrogenation over Ni/TiO₂ catalyst in vapour phase at atmospheric pressure: influence of preparation method. *Appl Petrochem Res* 6:15–23
- Kiasat AR, Zayadi M, Mohammad TF, Fallah MM (2011) Simple, practical and eco-friendly reduction of nitroarenes with zinc in the presence of polyethylene glycol immobilized on silica gel as a new solid-liquid phase transfer catalyst in water. *Iran J Chem Chem Eng* 30:37–41
- Lauwiner M, Rys P, Wissmann J (1998) Reduction of aromatic nitro compounds with hydrazine hydrate in the presence of an

- iron oxide hydroxide catalyst. I. The reduction of monosubstituted nitrobenzenes with hydrazine hydrate in the presence of ferrihydrite. *Appl Catal A-Gen* 172:141–148
- Sheng T, Qi YJ, Lin X, Hu P, Sun SG, Lin WF (2016) Insights into the mechanism of nitrobenzene reduction to aniline over Pt catalyst and the significance of the adsorption of phenyl group on kinetics. *Chem Eng J* 293:337–344
 - Zhou B, Song J, Zhou H, Wu L, Wu T, Liu Z, Han B (2015) Light-driven integration of the reduction of nitrobenzene to aniline and the transformation of glycerol into valuable chemicals in water. *RSC Adv* 5:36347–36352
 - Kumbhar PS, Sanchez-Valente J, Millet JMM, Figueras F (2000) Mg–Fe hydrotalcite as a catalyst for the reduction of aromatic nitro compounds with hydrazine hydrate. *J Catal* 191:467–473
 - Daems N, Wouters J, Van Goethem C, Baert K, Poleunis C, Delcorte A, Pescarmona PP (2018) Selective reduction of nitrobenzene to aniline over electrocatalysts based on nitrogen-doped carbons containing non-noble metals. *Appl Catal B-Env* 226:509–522
 - Formenti D, Ferretti F, Scharnagl FK, Beller M (2018) Reduction of nitro compounds using 3d-non-noble metal catalysts. *Chem Rev* 119:2611–2680
 - Krogul-Sobczak A, Cedrowski J, Kasperska P, Litwinienko G (2019) Reduction of Nitrobenzene to Aniline by CO/H₂O in the Presence of Palladium Nanoparticles. *Catalysts* 9:404
 - Sreenavya A, Baskaran T, Ganesh V, Sharma D, Kulal N, Sakthivel A (2018) Framework of ruthenium-containing nickel hydrotalcite-type material: preparation, characterisation, and its catalytic application. *RSC Adv* 8:25248–25257
 - Sreenavya A, Neethu PP, Sakthivel A (2021) The role of group VIII metals in hydro-conversion of lignin to value-added chemicals and biofuels. In: Pant KK, Gupta SK, Ahmed E (eds) *Catalysis for clean energy and environmental sustainability*. Springer Nature, Switzerland AG
 - Yan K, Liu Y, Lu Y, Chai J, Sun L (2017) Catalytic application of layered double hydroxide-derived catalysts for the conversion of biomass-derived molecules. *Catal Sci Technol* 7(8):1622–1645
 - Lucrédio AF, Assaf JM, Assaf EM (2014) Reforming of a model sulfur-free biogas on Ni catalysts supported on Mg (Al) O derived from hydrotalcite precursors: effect of La and Rh addition. *Biomass Bioenergy* 60:8–17
 - Basile F, Bersani I, Del Gallo P, Fiorilli S, Fornasari G, Gary D, Vaccari A (2011) In situ IR characterization of CO interacting with Rh nanoparticles obtained by calcination and reduction of hydrotalcite-type precursors. *Int J Spectroscopy*. <https://doi.org/10.1155/2011/458089>
 - Motokura K, Fujita N, Mori K, Mizugaki T, Ebitani K, Jitsukawa K, Kaneda K (2006) Environmentally friendly one-pot synthesis of α -alkylated nitriles using hydrotalcite-supported metal species as multifunctional solid catalysts. *Chem Eur J* 12(32):8228–8239
 - Seetharamulu P, Kumar VS, Padmasri AH, Raju BD, Rao KR (2007) A highly active nano-Ru catalyst supported on novel Mg–Al hydrotalcite precursor for the synthesis of ammonia. *J Mol Catal A-Chem* 263(1–2):253–258
 - Baskaran T, Mahato NR, Christopher J, Sakthivel A (2015) Cobalt-nanoparticles supported on mesoporous silica intercalated hydrotalcite (Co-MgAl-HT-SBA) prospective catalysts for hydroformylation. *Adv Porous Mater* 2(3):183–188
 - Baskaran T, Christopher J, Sakthivel A (2015) Progress on layered hydrotalcite (HT) materials as potential support and catalytic materials. *RSC Adv* 5(120):98853–98875
 - Baskaran T, Kumaravel R, Christopher J, Sakthivel A (2014) Silicate anion intercalated cobalt-aluminium hydrotalcite (CoAl-HT-Si): a potential catalyst for alcohol oxidation. *RSC Adv* 4(22):11188–11196
 - Baskaran T, Kumaravel R, Christopher J, Sakthivel A (2013) Silicate anion-stabilized layered magnesium–aluminium hydrotalcite. *RSC Adv* 3(37):16392–16398
 - Sociás-Viciano MM, Ureña-Amate MD, González-Pradas E, García-Cortés MJ, López-Teruel C (2008) Nitrate removal by calcined hydrotalcite-type compounds. *Clays Clay Miner* 56(1):2–9
 - Aramendía MA, Avilés Y, Benítez JA, Borau V, Jiménez C, Marinas JM, Urbano FJ (1999) Comparative study of Mg/Al and Mg/Ga layered double hydroxides. *Microporous Mesoporous Mater* 29(3):319–328
 - Hibino T, Tsunashima A (1997) Formation of spinel from a hydrotalcite-like compound at low temperature: reaction between edges of crystallites. *Clays Clay Miner* 45(6):842–853
 - Dębek R, Motak M, Duraczyska D, Launay F, Galvez ME, Grzybek T, Da Costa P (2016) Methane dry reforming over hydrotalcite-derived Ni–Mg–Al mixed oxides: the influence of Ni content on catalytic activity, selectivity and stability. *Catal Sci Technol* 6(17):6705–6715
 - Nawfal M, Gennequin C, Labaki M, Nsouli B, Aboukais A, Abi-Aad E (2015) Hydrogen production by methane steam reforming over Ru supported on Ni–Mg–Al mixed oxides prepared via hydrotalcite route. *Int J Hydrogen Energy* 40(2):1269–1277
 - Sreenavya A, Sahu A, Sakthivel A (2020) Hydrogenation of lignin-derived phenolic compound eugenol over ruthenium-containing nickel hydrotalcite-type materials. *Ind Eng Chem Res* 59(26):11979–11990
 - Cesar DV, Baldanza MA, Henriques CA, Pompeo F, Santori G, Múnera J, Nichio N (2013) Stability of Ni and Rh–Ni catalysts derived from hydrotalcite-like precursors for the partial oxidation of methane. *Int J Hydrogen Energy* 38(14):5616–5626
 - Miyata T, Shiraga M, Li D, Atake I, Shishido T, Oumi Y, Takehira K (2007) Promoting effect of Ru on Ni/Mg (Al) O catalysts in DSS-like operation of CH₄ steam reforming. *Catal Commun* 8(3):447–451
 - Martins JA, Faria A, Soria MA, Miguel CV, Rodrigues AE, Madeira LM (2019) CO₂ methanation over hydrotalcite-derived nickel/ruthenium and supported ruthenium catalysts. *Catalysts* 9(12):1008
 - Wierzbicki D, Baran R, Dębek R, Motak M, Grzybek T, Gálvez ME, Da Costa P (2017) The influence of nickel content on the performance of hydrotalcite-derived catalysts in CO₂ methanation reaction. *Int J Hydrogen Energy* 42(37):23548–23555
 - Freakley SJ, Ruiz-Esquius J, Morgan DJ (2017) The X-ray photoelectron spectra of Ir, IrO₂ and IrCl₃ revisited. *Surf Interface Anal* 49(8):794–799
 - Morgan DJ (2015) Resolving ruthenium: XPS studies of common ruthenium materials. *Surf Interface Anal* 47(11):1072–1079
 - Valdés-Martínez OU, Suárez-Toriello VA, De los Reyes JA, Pawelec B, Fierro JLG, (2017) Support effect and metals interactions for NiRu/Al₂O₃, TiO₂ and ZrO₂ catalysts in the hydrodeoxygenation of phenol. *Catal Today* 296:219–227
 - Daems N, Wouters J, Van Goethem C, Baert K, Poleunis C, Delcorte A, Pescarmona PP (2018) Selective reduction of nitrobenzene to aniline over electrocatalysts based on nitrogen-doped carbons containing non-noble metals. *Appl Catal B* 226:509–522
 - Datta KJ, Rathi AK, Kumar P, Kaslik J, Medrik I, Ranc V, Gawande MB (2017) Synthesis of flower-like magnetite nano-assembly: application in the efficient reduction of nitroarenes. *Sci Rep* 7(1):1–12
 - Blaser H (2006) A golden boost to an old reaction. *Science-New York Then Washington* 313:312
 - Yang XJ, Chen B, Zheng LQ, Wu LZ, Tung CH (2014) Highly efficient and selective photocatalytic hydrogenation of functionalized nitrobenzenes. *Green Chem* 16(3):1082–1086

38. Raj KJA, Prakash MG, Mahalakshmy R, Elangovan T, Viswanathan B (2012) Liquid phase hydrogenation of nitrobenzene over nickel supported on Titania. *Chinese J Catal* 33(7–8):1299–1305
39. Zhang J, Dong K, Luo W, Guan H (2018) Selective transfer hydrogenation of furfural into furfuryl alcohol on Zr-containing catalysts using lower alcohols as hydrogen donors. *ACS Omega* 3(6):6206–6216
40. Easterday R, Sanchez-Felix O, Losovyj Y, Pink M, Stein BD, Morgan DG, Rakitin M, Doluda VY, Sulman MG, Mahmoud WE (2015) Design of ruthenium/iron oxide nanoparticle mixtures for hydrogenation of nitrobenzene. *Catal Sci Technol* 5:1902–1910
41. Peureux J, Torres M, Mozzanega H, Giroir-Fendler A, Dalmon JA (1995) Nitrobenzene liquid-phase hydrogenation in a membrane reactor. *Catal Today* 25:409–415
42. Qu R, Macino M, Iqbal S, Gao X, He Q, Hutchings GJ, Sankar M (2018) Supported bimetallic AuPd nanoparticles as a catalyst for the selective hydrogenation of nitroarenes. *Nanomaterials* 8(9):690
43. Turáková M, Salmi T, Eränen K, Wärnå J, Murzin DY, Králik M (2015) Liquid phase hydrogenation of nitrobenzene. *Appl Catal A-Gen* 499:66–76
44. Lou BS, Veerakumar P, Chen SM, Veeramani V, Madhu R, Liu SB (2016) Ruthenium nanoparticles decorated curl-like porous carbons for high performance supercapacitors. *Scientific Rep* 6(1):1–11
45. Khan WU, Fakeeha AH, Al-Fatesh AS, Ibrahim AA, Abasaeed AE (2016) La₂O₃ supported bimetallic catalysts for the production of hydrogen and carbon nanomaterials from methane. *Int J Hydrogen Energy* 41(2):976–983
46. Awad A, Salam A (1891) Abdullah B (2017) Thermocatalytic decomposition of methane/methanol mixture for hydrogen production: Effect of nickel loadings on alumina support. *AIP Conf Proc* 1:020030. <https://doi.org/10.1063/1.5005363>

Publisher's Note Springer Nature remains neutral with regard to jurisdictional claims in published maps and institutional affiliations.

Authors and Affiliations

A. Sreenavya¹ · Shabas Ahammed¹ · Arya Ramachandran¹ · V. Ganesh² · A. Sakthivel¹ 

¹ Inorganic Materials & Heterogeneous Catalysis Laboratory, Department of Chemistry, School of Physical Sciences, Sabarmati Building, Tejaswini Hills, Central University of Kerala, Kasaragod 671320, India

² Electrodes and Electrocatalysis (EEC) Division, CSIR – Central Electrochemical Research, Institute (CSIR – CECRI), Karaikudi 630003, Tamil Nadu, India